DOI: 10.61782/fa.2023.0892

forum acusticum 2023

IDENTIFYING THE ACTIVE FLOW REGIONS IN ACOUSTIC-HYDRODYNAMIC FEEDBACK MECHANISMS

Javier Sierra-Ausin[1,2] **Flavio Giannetti**[2] **David Fabre**[1] **Felice Fruncillo**[2,3]

[1]IMFT, Institut de Mécanique des fluides de Toulouse, CNRS, Toulouse 31400, France
[2] Università degli Studi di Salerno - Via Giovanni Paolo II, 132, 84084 Fisciano, Italia
[3] Flight Dynamics and Simulation Laboratory, CIRA, Via Maiorise, 81043 Capua (CE)

ABSTRACT

Acoustic-hydrodynamic feedbacks are a common theme in jet noise. Strong sound emissions are supported by fluid instabilities, whose core is not necessarily localized in space. A common example is the feedback-loop instability of cavity flows, impinging jets or the flow past airfoils. The feedback-loop is composed of a convective instability, which is usually an instability of the shear layer, and an acoustic pressure wave or a hydrodynamic non-local effect. Despite the fact that such a mechanism is widely accepted, a precise identification of the most sensitive spatial regions underpinning the instability is missing. Herein, we propose a non-local decomposition of the structural sensitivity, which allows us to precisely identify the most sensitive regions of the flow responsible for the closure of the feedback-loop. The systematic use of these techniques could be applied in the design of passive flow control devices.

Keywords: *Instabilities, Non-local feedback, Structural sensitivity, Helmholtz decomposition.*

1. INTRODUCTION

Turbulent motion is ubiquitous in nature. While the vortex dynamics associated to turbulence necessarily involves a large range of scales, the large coherent structures supporting the fluid motion are commonly issued from a fluid instability. The nature of fluid instabilities is commonly classified as absolute and convective [1]. In the latter case (convectively unstable), the amplitude associated to the instability grows in a moving frame of reference, whereas in the former case (absolutely unstable) it grows at the very location of the source, and subsequently spreads elsewhere. Giannetti et al. [2] introduced the concept of *structural sensitivity* to identify the *wave-maker*, that is, the spatial region where the mechanism that sustains the instability is active. This concept was later generalised to include base-flow changes, saturation and non-linear effects [3–8]. While, for many fluid instabilities, the spatial distribution of the structural sensitivity is highly localised, e.g., the flow past a rotating particle [9] or the flow past a spinning cylinder [10], many other flow configurations exhibit fluid instabilities underpinned by a non-local feedback-loop. The high intensity tonal noise associated to cavity flows [11], impinging jets [12], the flow past airfoils [13] or the whistling of a jet past a thick hole [14, 15] is supported by an acoustic-hydrodynamic feedback. Herein, we propose a decomposition of the structural sensitivity tensor, which is not localised in space, to identify the *local wave-makers* composing the feedback loop. In the following, the methodology is introduced in the global linear stability framework [16], and the extension to a generic setting integrated by a time-stepping [17] will be the core of future studies.

*__Corresponding author__: javier.sierra@imft.fr.

2. METHODOLOGY

2.1 Linear stability

Herein, we introduce the linearised compressible Navier–Stokes equations in primitive variables $[\hat{\rho}, \hat{\mathbf{u}}, \hat{s}, \hat{T}, \hat{p}]^T$. The linearised equations are

$$\begin{aligned} &\Big(-\mathrm{i}\omega\mathbf{B}|_{\mathbf{q}_0} + \mathbf{DF}|_{\mathbf{q}_0}\Big)\hat{\mathbf{q}} = 0, \\ \text{with}\quad &\mathbf{B}|_{\mathbf{q}_0} = \mathrm{diag}(1, \rho_0\mathbf{I}, \rho_0 T_0, 0, 0), \end{aligned} \tag{2}$$

where the Jacobian operator $\mathbf{DF}|_{\mathbf{q}_0}$ is detailed in eq. (1). The primitive variables $[\hat{\rho}, \hat{\mathbf{u}}, \hat{s}, \hat{T}, \hat{p}]^T$ are the density, velocity, entropy, temperature and pressure fluctuations, respectively. The adjoint equations, on the other hand, read

$$\begin{aligned} &\Big(\mathrm{i}\overline{\omega}\mathbf{B}|_{\mathbf{q}_0} + \mathbf{DF}^\dagger|_{\mathbf{q}_0}\Big)\hat{\mathbf{q}}^\dagger = 0, \\ \text{with}\quad &\mathbf{B}|_{\mathbf{q}_0} = \mathrm{diag}(1, \rho_0\mathbf{I}, \rho_0 T_0, 0, 0), \end{aligned} \tag{3}$$

where the linear operator $\mathbf{DF}^\dagger|_{\mathbf{q}_0}$ is defined in eq. (4). We use an absorbing boundary condition, see fig. 1, named the complex mapping technique [18, 19] for both the direct and adjoint stability computations.

2.2 Decomposition of the perturbations

We first elaborate on the decomposition of the global mode $\hat{\mathbf{q}}$ into an *acoustic*, *hydrodynamic* and *entropic* component.

In particular, we adopt a Helmholtz-Hodge decomposition [20] of the perturbation velocity field into a *acoustic* (potential) and an *hydrodynamic* (solenoidal) part:

$$\hat{\mathbf{u}} = \hat{\mathbf{u}}_{\text{ac}} + \hat{\mathbf{u}}_{\text{hyd}} = \nabla\phi_c + \nabla\times\boldsymbol{\Psi}. \tag{5}$$

We obtain a Poisson problem after applying the divergence operator to eq. (5). In this case, the potential ϕ_c is a solution of the following Poisson equation

$$\begin{aligned} \Delta\phi_c &= \nabla\cdot\hat{\mathbf{u}} \quad \text{in } \Omega \\ \nabla\phi_c\cdot\mathbf{n} &= \hat{\mathbf{u}}\cdot\mathbf{n} \quad \text{on } \partial\Omega. \end{aligned} \tag{6}$$

The hydrodynamic component of the velocity is subsequently determined by subtracting $\hat{\mathbf{u}}_{\text{hyd}} = \hat{\mathbf{u}} - \hat{\mathbf{u}}_{\text{ac}} = \hat{\mathbf{u}} - \nabla\phi_c$. Alternatively, we could have determined first the stream function $\boldsymbol{\Psi}$, by taking the curl of eq. (5) and solving the subsequent vector-Poisson equation. The Helmholtz decomposition is not necessarily L^2-orthogonal, unless suitable boundary conditions are imposed to eq. (6). Herein, we adopt homogeneous boundary conditions at the far-field. The acoustic and hydrodynamic pressure components are retrieved by solving an elliptic problem resulting from the application of the divergence operator onto the linearised momentum equation, while only retaining the corresponding fluctuating velocity component, cf [21, Ch. 3]. The acoustic and hydrodynamic components of the fluctuating density and temperature are recovered by considering the isentropic relationship. Finally, the entropic component is retrieved by subtraction.

2.3 Identification of the underlying hydrodynamic-acoustic mechanism underpinning the feedback-loop

In cases where the global instability is the result of a long-range feedback-loop, e.g., the interaction between two travelling waves, a local definition of the wavemaker is not appropriate and the "active" region of the flow cannot be identified by the largest values of the *structural sensitivity* map. A further decomposition of fluctuating components and of the structural properties of the problem is required. Before, we introduce the *localised structural sensitivity*, we briefly recall the concept. The adjoint equations are herein used to evaluate the effect of a small "structural change" of the governing equation in the form of a linear harmonic term $\mathbf{H}(\hat{\mathbf{q}}) \equiv \delta(\mathbf{x}-\mathbf{x}_0)\mathbf{P}_{\mathbf{H}}\mathbf{C}_0\mathbf{P}_{\hat{\mathbf{q}}}\hat{\mathbf{q}}$,

$$\Big(-\mathrm{i}\omega\mathbf{B}|_{\mathbf{q}_0} + \mathbf{DF}|_{\mathbf{q}_0}\Big)\hat{\mathbf{q}} = \mathbf{H}(\hat{\mathbf{q}}). \tag{7}$$

$\mathbf{C}_0$ is a generic linear operator acting on $\hat{\mathbf{q}}$, and $\mathbf{P}_{\mathbf{H}}$ a diagonal matrix that selects the type of forcing (feedback). In the following, we neglect mass injection to the system, and we simply consider momentum forcing and a source of heat release, that is, $\mathbf{P}_{\mathbf{H}} = \mathrm{diag}(0, \mathbf{I}, 1, 0, 0)$. The projection operator $\mathbf{P}_{\hat{\mathbf{q}}}$ is also a diagonal matrix that selects the dependency of the forcing on the perturbation. The change in the eigenvalue produced by the "structural" change of the operator is thus expressed as

$$\begin{aligned} \mathrm{i}\delta\omega &= \langle \mathbf{P}_{\mathbf{H}}\hat{\mathbf{q}}^\dagger, \delta(\mathbf{x}-\mathbf{x}_0)\mathbf{C}_0\mathbf{P}_{\hat{\mathbf{q}}}\hat{\mathbf{q}}\rangle \\ &\le ||\mathbf{C}_0||||\mathbf{P}_{\mathbf{H}}\hat{\mathbf{q}}^\dagger||_{L^2}||\mathbf{P}_{\hat{\mathbf{q}}}\hat{\mathbf{q}}||_{L^2} \\ &= ||\mathbf{C}_0||||\mathbf{S}_s(\mathbf{x}_0)||_F, \end{aligned} \tag{8}$$

while the structural sensitivity tensor is defined as $\mathbf{S}_s(\mathbf{x}_0) \equiv \mathbf{P}_{\mathbf{H}}\hat{\mathbf{q}}^\dagger \otimes \mathbf{P}_{\hat{\mathbf{q}}}\hat{\mathbf{q}}$. The Frobenius norm of this tensor $||\mathbf{S}_s(\mathbf{x}_0)||_F \equiv ||\mathbf{P}_{\mathbf{H}}\hat{\mathbf{q}}^\dagger||_{L^2}||\mathbf{P}_{\hat{\mathbf{q}}}\hat{\mathbf{q}}||_{L^2}$ is usually referred to as the structural sensitivity map. The decomposition of the feedback term allows us to introduce a novel

$$\mathbf{DF}|_{\mathbf{q}_0}\hat{\mathbf{q}} = \begin{cases} \mathbf{u}_0\cdot\nabla\hat{\rho} + \hat{\rho}\nabla\cdot\mathbf{u}_0 + \hat{\mathbf{u}}\cdot\nabla\rho_0 + \rho_0\nabla\cdot\hat{\mathbf{u}} & \text{(1a)} \\ \hat{\rho}\mathbf{u}_0\cdot\nabla\mathbf{u}_0 + \rho_0\mathbf{u}_0\cdot\nabla\hat{\mathbf{u}} + \rho_0\hat{\mathbf{u}}\cdot\nabla\mathbf{u}_0 + \nabla\hat{p} - \dfrac{1}{\mathrm{Re}}\nabla\cdot\tau(\hat{\mathbf{u}}) & \text{(1b)} \\ \quad -\gamma(\gamma-1)\dfrac{M_\infty^2}{\mathrm{Re}}\big(\tau(\hat{\mathbf{u}}):\mathbf{D}(\mathbf{u}_0) + \tau(\mathbf{u}_0):\mathbf{D}(\hat{\mathbf{u}})\big) - \dfrac{\gamma}{\mathrm{Pr\,Re}}\Delta\hat{T} & \\ \quad +\rho_0 T_0\mathbf{u}_0\cdot\nabla\hat{s} + \rho_0 T_0\hat{\mathbf{u}}\cdot\nabla s_0 + \hat{\rho}T_0\mathbf{u}_0\cdot\nabla s_0 + \rho_0\hat{T}\mathbf{u}_0\cdot\nabla s_0 & \text{(1c)} \\ \rho_0 T_0\hat{s} + (\gamma-1)T_0\hat{\rho} - \rho_0\hat{T} & \text{(1d)} \\ \quad -\rho_0\hat{T} - \hat{\rho}T_0 + \gamma M_\infty^2\hat{p} & \text{(1e)} \end{cases}$$

$$\mathbf{DF}^\dagger|_{\mathbf{q}_0}\hat{\mathbf{q}}^\dagger = \begin{cases} -\mathbf{u}_0\cdot\nabla\hat{\rho}^\dagger + \big(\mathbf{u}_0\cdot\nabla\mathbf{u}_0\big)\cdot\hat{\mathbf{u}}^\dagger + (\mathbf{u}_0\cdot\nabla s_0)\hat{s}^\dagger + T_0\big((\gamma-1)\hat{T}^\dagger - \hat{p}^\dagger\big) & \text{(4a)} \\ \quad -\rho_0\mathbf{u}_0\cdot\nabla\hat{\mathbf{u}}^\dagger + \rho_0\hat{\mathbf{u}}^\dagger\cdot(\nabla\mathbf{u}_0)^T - \dfrac{1}{\mathrm{Re}}\nabla\cdot\tau(\hat{\mathbf{u}}^\dagger) & \\ -\rho_0\nabla\hat{\rho}^\dagger + 2\gamma(\gamma-1)\dfrac{M_\infty^2}{\mathrm{Re}}\nabla\cdot(\hat{s}^\dagger\tau(\mathbf{u}_0)) + \rho_0 T_0\hat{s}^\dagger\nabla s_0 & \text{(4b)} \\ \quad -\rho_0 T_0\mathbf{u}_0\cdot\nabla\hat{s}^\dagger + \rho_0 T_0\hat{T}^\dagger & \text{(4c)} \\ \rho_0 T_0\hat{s}^\dagger\mathbf{u}_0\cdot\nabla s_0 - \dfrac{\gamma}{\mathrm{Pr\,Re}}\nabla^2\hat{s}^\dagger - \rho_0\hat{p}^\dagger - \rho_0\hat{T}^\dagger & \text{(4d)} \\ \gamma M_\infty^2\hat{p}^\dagger - \nabla\cdot\hat{\mathbf{u}}^\dagger & \text{(4e)} \end{cases}$$

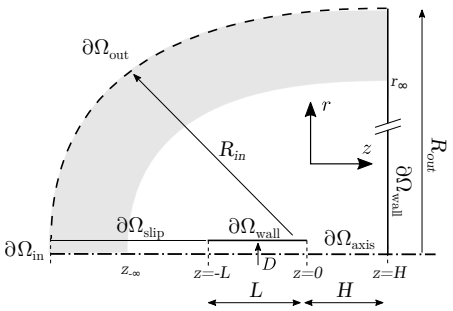

Figure 1: Diagram of the computational domain of the rounded impinging jet configuration. The physical domain, represented as a white area, is complemented with a radial absorbing layer (CM), shown as a light grey shaded zone.

definition of a *localised structural sensitivity* matrix as

$$\begin{aligned} \mathrm{i}\delta\omega_j^k &= \langle\hat{\mathbf{q}}_k^\dagger, \delta(\mathbf{x}-\mathbf{x}_0)\mathbf{C}_0\hat{\mathbf{q}}_j\rangle \\ &\leq ||\mathbf{C}_0||||\hat{\mathbf{q}}_k^\dagger(\mathbf{x}_0)||||\hat{\mathbf{q}}_j(\mathbf{x}_0)|| \\ &= ||\mathbf{C}_0||||\mathbf{S}^{(j,k)}{}_s(\mathbf{x}_0)||_F, \end{aligned} \tag{9}$$

where the localised structural sensitivity tensor is defined as

$$\mathbf{S}^{(j,k)}{}_s(\mathbf{x}_0) = \mathbf{P}_{\mathbf{H}}\hat{\mathbf{q}}_k^\dagger(\mathbf{x}_0)\otimes\mathbf{P}_{\hat{\mathbf{q}}}\hat{\mathbf{q}}_j(\mathbf{x}_0) \tag{10}$$

with j and k chosen among $\{\mathrm{ac}, \mathrm{hyd}, \mathrm{s}\}$. In particular, the new *structural sensitivity* can provide information about the cross-interaction between vortical and acoustic components of the flow.
Without further discussion, we propose the following de-

composition of the adjoint mode,

$$\begin{aligned}
\hat{\mathbf{u}}^\dagger &= \hat{\mathbf{u}}^\dagger_{\text{hyd}} + \hat{\mathbf{u}}^\dagger_{\text{ac}} = \nabla\phi^\dagger_c + \nabla\times\boldsymbol{\Psi}^\dagger,\\
\hat{s}^\dagger &= \hat{s}^\dagger_{\text{s}}\\
\hat{\rho}^\dagger &= \hat{\rho}^\dagger_{\text{ac}} + \hat{\rho}^\dagger_{\text{hyd}} + \hat{\rho}^\dagger_{\text{s}},\\
\hat{p}^\dagger &= \hat{p}^\dagger_{\text{ac}} = \frac{\nabla\cdot\hat{\mathbf{u}}^\dagger}{\gamma M^2_\infty}\\
\hat{T}^\dagger &= \hat{T}^\dagger_{\text{ac}} + \hat{T}^\dagger_{\text{s}}\\
&= \left(\hat{s}^\dagger\mathbf{u}_0\cdot\nabla s_0 - \frac{\gamma}{\text{Pr Re}}\frac{\Delta\hat{s}^\dagger}{\rho_0}\right) - \frac{\nabla\cdot\hat{\mathbf{u}}^\dagger}{\gamma M^2_\infty}.
\end{aligned} \tag{11}$$

which allows us to evaluate quantitatively the interaction among the different components.

3. NUMERICAL EXAMPLE: ROUNDED IMPINGING JET

Herein, we apply the previously introduced concept of the localised structural sensitivity for the case of a rounded impinging jet, sketched in fig. 1. The decomposed structural sensitivity map is displayed in fig. 2 for two different Mach numbers of the jet (M_J). In the problem of the impinging jet, the feedback loop is initiated by the hydrodynamic instability of the shear layer (a Kelvin-Helmholtz wave), which induces an acoustic response (a backward wave) when it reaches the impinging region. In turn, when the generated acoustic wave impinges on the nozzle lip promotes back the hydrodynamic instability, continuing the loop. With the novel definition, $\mathbf{S}_s^{(hyd,ac)}$ identifies the most sensitive region of the flow where vortical perturbations induce an acoustic response, see fig. 2 (a-b). This region for the impinging jet is expected to be located near the wall and possibly near sharp corners. The second (and third) wavemaker of interest corresponds to the excitation of a hydrodynamic response from hydrodynamic ($\mathbf{S}_s^{(hyd,hyd)}$) or acoustic perturbations ($\mathbf{S}_s^{(ac,hyd)}$), the latter being displayed in fig. 2 (c-d). Physically, $\mathbf{S}_s^{(hyd,hyd)}$ determines the hydrodynamic wavemaker, which in a causal reasoning, could be argued to be the region initiating the feedback process, while $\mathbf{S}_s^{(ac,hyd)}$ determines the most sensitive region of the flow where an acoustic perturbation induces a hydrodynamic excitation, that is, the retroaction of the acoustic wave into the hydrodynamic instability.

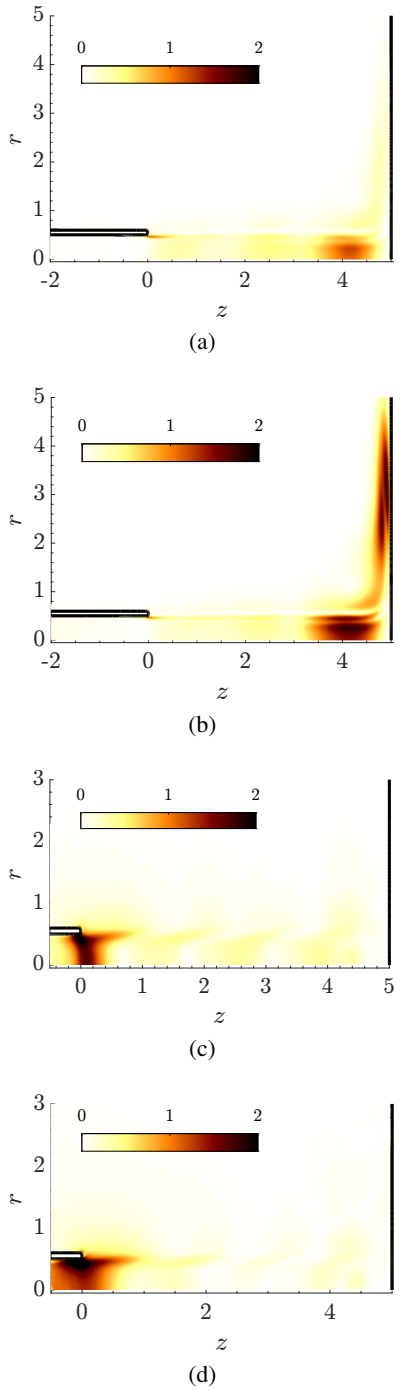

Figure 2: (a-b) Map $\mathbf{S}_s^{(hyd,ac)}$ for a global mode at (a) $M_J \approx 0.9$ and (b) $M_J \approx 0.5$. (c-d) Map $\mathbf{S}_{\mathbf{u},s}^{(ac,hyd)}$ for a global mode at (a) $M_J \approx 0.9$ and (b) $M_J \approx 0.5$.

4. REFERENCES

[1] P. Huerre and P. A. Monkewitz, "Local and global instabilities in spatially developing flows," *Annual re-*

view of fluid mechanics, vol. 22, no. 1, pp. 473–537, 1990.

[2] F. Giannetti and P. Luchini, "Structural sensitivity of the first instability of the cylinder wake," *Journal of Fluid Mechanics*, vol. 581, pp. 167–197, 2007.

[3] O. Marquet, D. Sipp, and L. Jacquin, "Sensitivity analysis and passive control of cylinder flow," *Journal of Fluid Mechanics*, vol. 615, p. 221–252, 2008.

[4] F. Giannetti, S. Camarri, and P. Luchini, "Structural sensitivity of the secondary instability in the wake of a circular cylinder," *Journal of Fluid Mechanics*, vol. 651, pp. 319–337, 2010.

[5] O. Marquet and L. Lesshafft, "Identifying the active flow regions that drive linear and nonlinear instabilities," *arXiv preprint arXiv:1508.07620*, 2015.

[6] F. Giannetti, S. Camarri, and V. Citro, "Sensitivity analysis and passive control of the secondary instability in the wake of a cylinde," *Journal of Fluid Mechanics*, vol. 864, pp. 45–72, 2019.

[7] J. Sierra, P. Jolivet, F. Giannetti, and V. Citro, "Adjoint-based sensitivity analysis of periodic orbits by the fourier–galerkin method," *Journal of Computational Physics*, vol. 440, p. 110403, 2021.

[8] J. Sierra-Ausin, V. Citro, F. Giannetti, and D. Fabre, "Efficient computation of time-periodic compressible flows with spectral techniques," *Computer Methods in Applied Mechanics and Engineering*, vol. 393, p. 114736, 2022.

[9] J. Sierra-Ausín, M. Lorite-Díez, J. Jiménez-González, V. Citro, and D. Fabre, "Unveiling the competitive role of global modes in the pattern formation of rotating sphere flows," *Journal of Fluid Mechanics*, vol. 942, p. A54, 2022.

[10] J. Sierra, D. Fabre, V. Citro, and F. Giannetti, "Bifurcation scenario in the two-dimensional laminar flow past a rotating cylinder," *Journal of Fluid Mechanics*, vol. 905, 2020.

[11] S. Yamouni, D. Sipp, and L. Jacquin, "Interaction between feedback aeroacoustic and acoustic resonance mechanisms in a cavity flow: a global stability analysis," *Journal of Fluid Mechanics*, vol. 717, pp. 134–165, 2013.

[12] M. Varé and C. Bogey, "Generation of acoustic tones in round jets at a mach number of 0.9 impinging on a plate with and without a hole," *Journal of Fluid Mechanics*, vol. 936, 2022.

[13] M. F. de Pando, P. J. Schmid, and D. Sipp, "A global analysis of tonal noise in flows around aerofoils," *Journal of Fluid Mechanics*, vol. 754, pp. 5–38, 2014.

[14] J. Sierra-Ausin, D. Fabre, V. Citro, and F. Giannetti, "Acoustic instability prediction of the flow through a circular aperture in a thick plate via an impedance criterion," *Journal of Fluid Mechanics*, vol. 943, p. A48, 2022.

[15] L. Hirschberg, J. G. Guzman Inigo, A. Aulitto, J. Sierra, D. Fabre, A. Morgans, and A. Hirschberg, "Linear theory and experiments for laminar bias flow impedance: Orifice shape effect," in *28th AIAA/CEAS Aeroacoustics 2022 Conference*, p. 2887, 2022.

[16] D. Fabre, V. Citro, D. Sabino, P. Bonnefis, J. S. Ausin, F. Giannetti, and M. Pigou, "A practical review on linear and nonlinear global approaches to flow instabilities," *Applied Mechanics Reviews*, vol. 70, no. 6, p. 060802, 2018.

[17] V. Citro, F. Giannetti, and J. Sierra, "Optimal explicit runge-kutta methods for compressible navier-stokes equations," *Applied Numerical Mathematics*, vol. 152, pp. 511–526, 2020.

[18] J. Sierra, D. Fabre, and V. Citro, "Efficient stability analysis of fluid flows using complex mapping techniques," *Computer Physics Communications*, vol. 251, p. 107100, 2020.

[19] J. Sierra, V. Citro, and D. Fabre, "On boundary conditions for compressible flow simulations," in *Fluid-Structure-Sound Interactions and Control: Proceedings of the 5th Symposium on Fluid-Structure-Sound Interactions and Control 5*, pp. 335–340, Springer, 2021.

[20] S. Schoder, K. Roppert, and M. Kaltenbacher, "Helmholtz's decomposition for compressible flows and its application to computational aeroacoustics," *SN Partial Differential Equations and Applications*, vol. 1, no. 6, pp. 1–20, 2020.

[21] J. Sierra-Ausin, *Mode interaction in external flows*. PhD thesis, 2023.